

Human Biophysics as Network Weights: Conditional Generative Models for Dynamic Simulation

Shihan Ma^{1,2}, Alexander Kenneth Clarke¹, Kostiantyn Maksymenko³, Samuel Deslauriers-Gauthier^{3,4}, Xinjun Sheng^{2,5}, Xiangyang Zhu^{2,5}, and Dario Farina¹

¹Department of Bioengineering, Imperial College London, London, UK; ²State Key Laboratory of Mechanical System and Vibration, Shanghai Jiao Tong University, Shanghai, China; ³Neurodec, Sophia Antipolis, France; ⁴Inria Centre at Université Côte d'Azur, Nice, France; ⁵Meta Robotics Institute, Shanghai Jiao Tong University, Shanghai, China

Simulations of biophysical systems have provided a huge contribution to our fundamental understanding of human physiology and remain a central pillar for developments in medical devices and human machine interfaces. However, despite their successes, such simulations usually rely on highly computationally expensive numerical modelling, which is often inefficient to adapt to new simulation parameters. This limits their use in simulating dynamic human behaviours, which typically proceed along a sequence of small time steps. One may painstakingly produce a few static simulations at discretised stages, but not the hundreds of simulations that are essential to capture the dynamic nature of human body. We propose that an alternative approach is to use conditional generative models, which can learn complex relationships between the underlying generative conditions and the output data whilst remaining inexpensive to sample from. As a demonstration of this concept, we present BioMime, a hybrid-structured generative model that combines elements of deep latent variable models and conditional adversarial training. We demonstrate that BioMime can learn to accurately mimic a complex numerical model of human muscle biophysics and then use this knowledge to continuously sample from a dynamically changing system in a short time. This ultimately converts a static model into a dynamic one with no effort. We argue that transfer learning approaches with conditional generative models are a viable solution for dynamic simulation with any numerical model.

conditional generative model | transfer learning | biophysical simulation | neurophysiology | electromyography

*

Biophysical simulations are a cornerstone of modern biomedical research and engineering, allowing initial exploration of experimental hypotheses and fast iteration of designs prior to physical implementation (1, 2). Decades of continuous developments have seen such models go from a few equations, such as in Hodgkin and Huxley's hugely impactful work on spiking neurons (3), to highly complex physics engines and large numerical models with thousands of individual parameters (4). The rapid expansion in the complexity and fidelity of biophysical simulations has played a major role in advancing their corresponding domains (5), and has even generated entirely new avenues of investigation, such as neurophysiological source reconstruction and embodied artificial intelligence (6, 7).

Despite their successes, the increasing complexity of biophysical simulations has come with a corresponding increase in the associated computational burden, which often limits adoption (5). Computational complexity is particularly problematic when simulating a dynamic event which rapidly changes the modelling conditions, for example the deformation of the volume conductor in a moving forearm (8), or the changes in

mechanical response of the tendons in a bending knee (9). Usually, the only solution to these types of problem is to discretise time, splitting one dynamic simulation into many individual static simulations, a task which is often computationally demanding or even unfeasible. A related issue is that adapting the model to new sets of parameters, such as a new individual, means that the model needs to be rerun with every parameter updated (10), which is a major barrier to the promised "digital twin" of personalised healthcare simulations (11).

We propose that a better approach to modelling dynamic human systems is to combine transfer learning approaches with conditional generative models (12). Specifically, the generative models are trained with a numerical simulation's outputs and then used to predict the emissions of the interpolated system states. Such a model could generate samples inexpensively for a variety of static simulations, or continually morph the emissions of an evolving dynamic state. To achieve these aims, we propose BioMime, an AI model that embeds a biophysical system into the weights of a neural network. Compared with the numerical model that takes the role of a teacher, BioMime manifests two main benefits. First, by implicitly learning the

Significance Statement

Simulations of biophysical systems are fundamental for studying physiological mechanisms and developing algorithms for biological information extraction. Whilst advanced numerical methods provide accurate static simulation models, they are computationally so expensive that they become prohibitive for simulating dynamic events. However, all biophysical systems have dynamic behaviour. We demonstrate that deep conditional generative models can replicate dynamic biophysical systems by learning from the static emissions of numerical models. A well-trained generative model can rapidly predict the outputs of a dynamic system by implicitly interpolating the system states in arbitrary temporal resolution. The proposed model enables an accurate, ultra-fast, and high temporal-resolution simulation of biophysical systems during dynamic changes. The model has wide applications in physiological and clinical research for uni/multidomain simulations.

S.M., A.K.C. and D.F. designed research; S.M., A.K.C., and D.F. performed research; S.M., K.M., and S.D. prepared dataset; S.M., A.K.C., and D.F. analysed data; X.S., X.Z., and D.F. supervised research; and S.M., A.K.C., and D.F. wrote the paper.

K.M. and S.D. are cofounders of company neurodec.

¹S.M. contributed equally to this work with A.K.C.

²To whom correspondence should be addressed. E-mail: d.farina@imperial.ac.uk and mexyzhu@sjtu.edu.cn

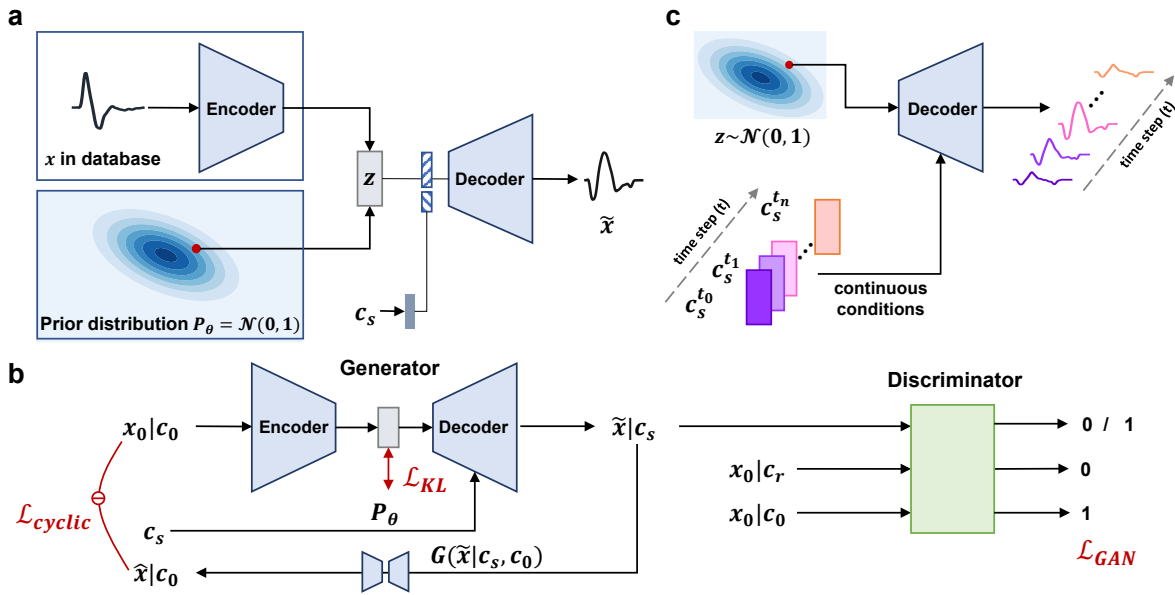


Fig. 1. Deep latent variable model, BioMime. **a**, The generative architecture of BioMime model. BioMime consists of an encoder and a conditional decoder. The decoder takes either an encoded latent or a standard normal sample as an input z and outputs an emission \tilde{x} . The output \tilde{x} reflects the learned generative factors of the desired biophysical system state, the specified conditions c_s . The encoder is particularly useful when the objective is to conditionally modify the input data whilst retaining the generative effects of unspecified generative factors. **b**, BioMime is trained with an adversarial loss \mathcal{L}_{GAN} using a discriminator which seeks to distinguish between the generated emissions \tilde{x} and the emissions of the numerical simulator x_0 . Like the decoder, the discriminator is also conditioned on c_s when given samples from the generator or the numerical simulator, meaning the generator must learn a conditional implicit density. To further drive conditional behaviour in the discriminator, the emissions of the numerical simulator x_0 are paired with specified conditions which are either correct c_0 or incorrect c_r . To allow for *ab initio* generation and to stabilise training, an additional Kullback-Leibler divergence \mathcal{L}_{KL} term is minimised between z and a standard normal prior. Finally we found empirically that the addition of a cycle-consistency loss \mathcal{L}_{cyclic} improved training stability and gave an increase in model performance (Supplementary Fig. 4). **c**, Rapid generation of a dynamically evolving emission *ab initio*. A sample is taken from the prior and then continuously transformed over time using a sweep of the specified conditions.

generative properties of the teacher simulation, BioMime can quickly expand the data space by interpolating system states. Second, once trained, BioMime is efficient in synthesising new data in real time, essentially converting the static numerical model into a dynamic one.

BioMime takes the form of a semi-supervised conditional deep latent variable model with an encoder-decoder structure. The encoder takes the numerical emissions and learns a compressed latent representation. The decoder reconstructs a new emission from the latent and the desired simulation parameters (Fig. 1a). This structure allows the model to accurately mimic a simulation's internal state and then generate emissions that replicate a dynamic change in that state. BioMime can also generate realistic samples *ab initio* without using an encoded representation by sampling from a prior. This is achieved by minimising the Kullback-Leibler (KL) divergence between the sufficient statistics extracted from the latent representation and a gaussian prior (13). With the above architectures, we demonstrated that training BioMime adversarially using a conditional discriminator (14, 15) contributes to the accurately synthesised emissions that are highly consistent with the numerical ground truths. We further proved that the high accuracy is preserved while interpolating the system states and only begins to decrease when the extrapolated states are largely deviated from the original data space. BioMime is two orders of magnitude faster than the state-of-the-art numerical model when generating the same amount of data. This allows it to quickly construct a dynamic simulation with high temporal resolution by continuously changing the input parameters. We finally showed an example using BioMime to synthesise

the changing electrical potentials during the dynamic contractions of a human forearm, which matches the biomechanical movements of a musculoskeletal model.

Results

BioMime accurately mimics computationally expensive models. To demonstrate the ability of BioMime to capture a complex biophysical model, BioMime was trained to replicate an advanced numerical volume conductor model, which is used for generating surface electromyographic (sEMG) signals. Surface EMG is a typical example of neurophysiological signals, consisting of repetitive spiking sources with linearly superposed electrical potentials (16). It provides non-invasive information on neural activities and is commonly used for clinical/biomedical applications and human machine interfaces (17–20). Modelling sEMG signals helps to uncover the underlying mechanisms of electrical potential field generation and propagation within human body and provides annotated dataset for training and validating signal processing techniques (21, 22).

Whilst numerical models of surface EMG generation have become highly advanced, they incur a huge computational burden when simulating the dynamic contractions, as the internal states of the model need to be continuously recalculated. This has proven to be a hindrance to the development of inverse models which can manage dynamic changes in the muscle (23), such as signals from a moving forearm used for prosthesis control. We proved that the proposed conditional generative model, BioMime, can learn from the teacher numerical model and accurately replicate the outputs of the numerical model.

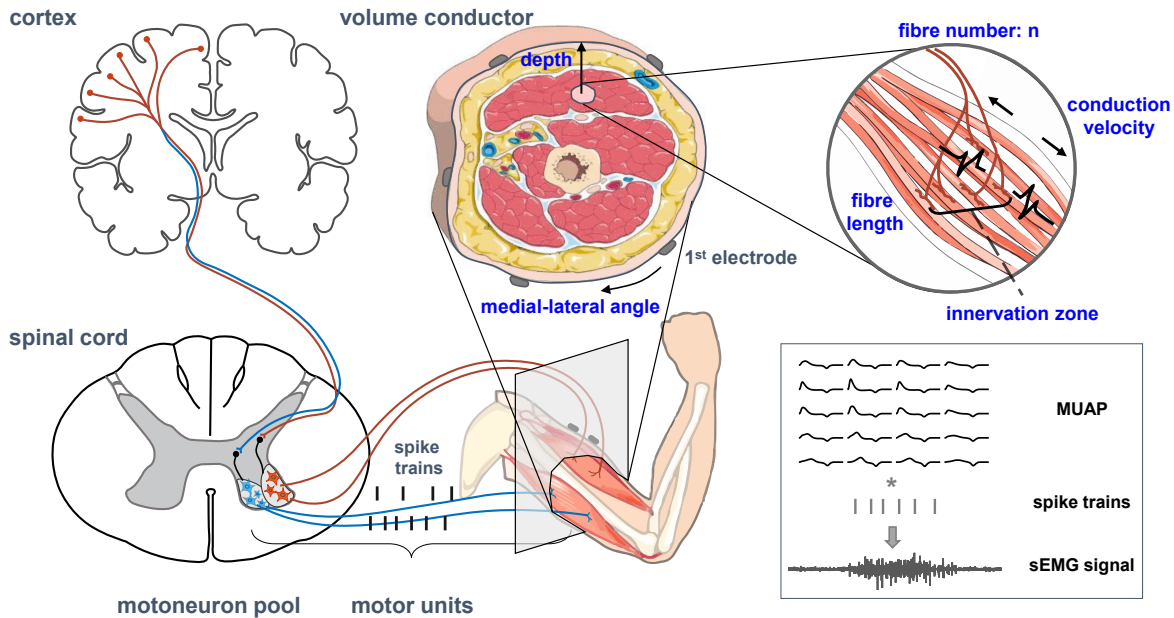


Fig. 2. Capturing a complex biophysical simulation. The effectiveness of BioMime is validated on a simulation of surface electromyogram (sEMG) signals recorded from a forearm. The sEMG signals represent the myoelectric output of motor neuron activities from the spinal cord and are detected by an array of electrodes placed on the skin above the muscles. Each spike from a specific motor neuron activates an associated pool of muscle fibres, where the combination of the motor neuron and the muscle fibres it controls is called a motor unit. The electrical potential field caused by the muscle activities is filtered by the volume conductor and sensed at the surface electrodes as the motor unit action potential (MUAP). Simulated MUAPs are convolved with the desired spike activities and then summed (with optional added gaussian noise) to build the simulated sEMG. For the emissions of the numerical simulation used to train BioMime, the bulk of MUAP variance is explained by six specified generative factors (highlighted in blue). These six factors are the specified conditions in the case of MUAP simulation.

The advanced numerical model we used to validate BioMime uses a finite element method to simulate motor unit action potentials (MUAPs), the basic component of EMG signal (22). As shown in Fig. 2, the shape of each MUAP waveform is dependent on a number of specified conditions, such as the location of the muscle fibres in the forearm (Fig. 3a). BioMime was trained using a set of MUAP emissions from the numerical simulator, with each waveform labelled with the specific conditions used to generate it. A held-out test set of emissions was used to validate the model, which was done by taking a MUAP emission from the numerical simulator and using BioMime to transform the emission conditioned on another set of parameters. The output of BioMime was then compared to the equivalent emission from the simulator. BioMime was able to consistently and accurately transform MUAPs based on the specified conditions, generating waveforms which were extremely similar in shape to the simulation equivalent (Fig. 3b). The mean normalised root mean square error (nRMSE) across all samples was 1.8% when evaluated on the held-out test set and there was equal performance across all six of the specified conditions (Fig. 3c).

An interesting result of conditioning the decoder is that the encoder outputs tended to lose the information about the specified conditions, analogous to semi-supervised disentanglement methods (24, 25). We investigated this effect with an informativeness metric (26), which measures how much information of the specified conditions are contained within the latent features. A non-linear regressor was used to inversely predict the specified conditions from the encoded waveform. We found that the latent features held very little information about the specified conditions, with a median informativeness score slightly above chance at 35.9% (Supplementary Table

2). This low informativeness metric indicates that the generative effects of the specified conditions were disentangled from those that were unspecified, i.e., not explicitly included during training. We speculate that this disentanglement improves the predictability of the model responses to the changes in the specified conditions by reducing the burden on the decoder.

Predicting the emissions of a dynamically evolving system.

To prove that BioMime could conditionally transform MUAPs by accurately interpolating among the internal states of the numerical simulator, we transformed MUAPs for all samples in the test dataset according to a sweep of the specified conditions. Three sets of conditions within the sweep matched the numerical dataset at equal distances along the swept paths. In other words, there were three ground truths that we can compare BioMime's outputs to. As shown in Fig. 4a, the simulated MUAPs changed continuously with the conditions and accurately matched the three ground truth MUAPs. The temporal resolution of the interpolation can be super high by simply increasing the number of time steps.

As the specified conditions moved further away from the original values used to generate the waveform, the MUAP shape increasingly deviated away from the ground truth. However, the discrepancy was not large (nRMSE less than 2.0%) until the sweep intersected with the third ground truth (Fig. 4b), which was the sample with the generative factors most different from the original point. This means that even for situations where very high interpolation accuracies are desired during a dynamic traversal, a relatively small dataset from the computational expensive numerical simulator is sufficient.

We further visualised the distributions of the original dataset, interpolated BioMime transformations, and extrapo-

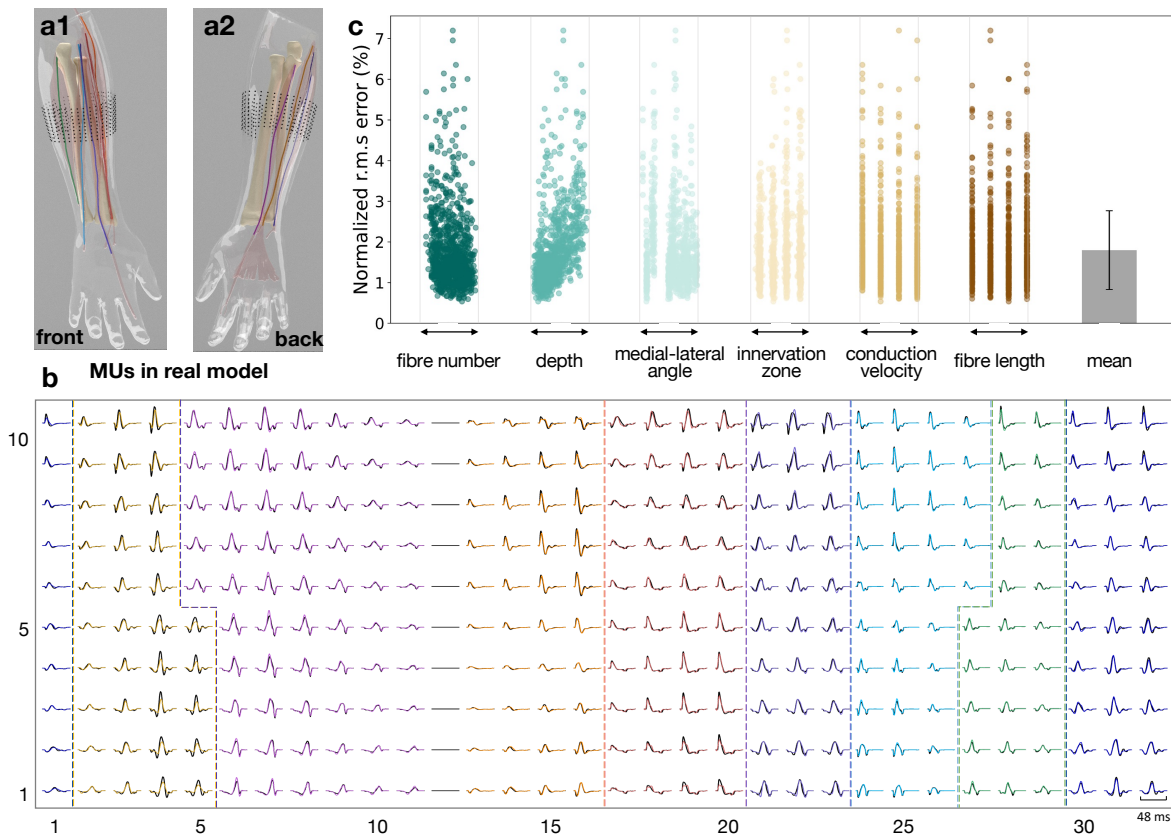


Fig. 3. BioMime accurately learns to mimic a biophysical simulation. **a**, Muscle fibre locations of the eight representative motor units (MUs) highlighted in different colors from front and back. Each MU is from a separate muscle in the realistic forearm volume conductor. The black dots represent the surface electrode array with 10×32 channels and the inter-electrode distance is 8 mm. **b**, MUAP signals synthesised by conditionally transforming the action potentials of the eight MUs in **a**, compared with the ground truth in black lines. For each MU, only channels with large amplitudes are illustrated in sub-grids. These channels represent the electrodes that are physically closest to the MU. Sub-grids from different MUs are separated by dotted lines. The numbers beside and below the grid denote the indices of electrodes in row and in column, respectively. The shape of each transformed MUAP from BioMime closely matches its simulated counterpart. **c**, Normalised root mean square error in percentage between the emissions from BioMime and those from the numerical simulator across the six specified conditions and overall evaluated on the held-out test set. The normalised range of each condition's values is represented on the x-axis. The effect of all of the specified conditions on the simulation emissions was closely mimicked by BioMime.

lated BioMime transformations by using t-distributed stochastic neighbor embedding (t-SNE) dimensionality reduction (27) in Fig. 4c. The samples in the original dataset were grouped into small clusters, as the MUAPs in each muscle were highly similar. The waveforms generated by interpolating the specified conditions closely matched the distribution of the MUAPs from the original simulation. MUAPs generated by BioMime using specified conditions outside of those in the training set generally remained close to the original distribution until the specified conditions had deviated by a relative difference greater than 60%. This again demonstrates that BioMime is able to expand the data space whilst keeping the generation accuracy as well.

Inexpensively simulating a dynamic human biophysical system. Once trained, BioMime is able to rapidly generate emissions using any variety of specified conditions. Synthesising 3,200 MUAPs under 1,000 continuous conditions only takes around 80 seconds, which is two orders of magnitude faster than the state-of-the-art numerical model (22). The low computational burden allows BioMime to produce continuous emissions of signals that capture the dynamics of the physical system. This is easily superior to traditional numerical methods, as adapting the finite element model to new param-

eters requires complex integration of several pre-processing steps, which is extremely time-demanding and computationally expensive (8, 28).

To demonstrate the utility of BioMime as a method of converting a static biophysical simulation into a dynamic one, the trained model was used to simulate sEMG signals from the outputs of a musculoskeletal model during finger and wrist movements (Fig. 5). We defined the movements of the musculoskeletal model by interpolating between four gestures, including palm extension, hand grasp, wrist flexion, and wrist extension (Fig. 5a). Details of the musculoskeletal model are described in *Methods*. MUAPs from the eight forearm muscles in the numerical dataset were continuously transformed given the muscle length profiles from the musculoskeletal model. As only one specified condition, the muscle length, was changed during the transformation, the variation in the MUAP waveforms is mainly reflected in the duration of the waveform and the end-fibre effects, a complex interaction that is correctly predicted by BioMime (Fig. 5b).

The library of the transformed MUAPs was then convolved with a set of motor neuron spike trains that represent a trapezoidal activation of flexors and extensors (Fig. 5d). We used trapezoidal activation since it is commonly used in the

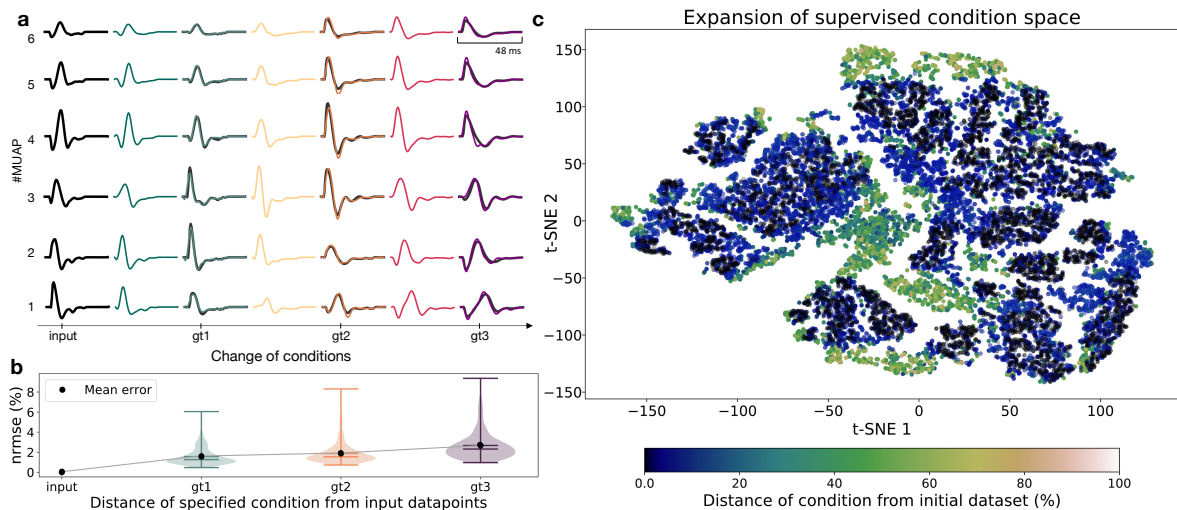


Fig. 4. BioMime can predictively interpolate and extrapolate between simulation conditions and beyond. **a**, A set of BioMime-transformed MUAPs sampled from a continuous sweep of specified conditions. The original MUAPs in the dataset were encoded and then continuously transformed away from their origins (x-axis tick label of 'input'). As the specified conditions were continuously traversed, they occasionally intersected with the generative factors from the numerical simulator (displayed as superimposed black lines, x-axis tick labels of 'gt1', 'gt2', and 'gt3'), which can be used as a ground truth. **b**, Mean normalised root mean squared error of the BioMime-transformed MUAPs compared to their ground truth counterparts from the test set during the traversal in **a**. The predictive error of BioMime increased as the specified conditions moved further away from their origin. BioMime is able to compensate for large moves away from the original conditions before the error starts to rise. **c**, A t-SNE projection of the MUAP emissions from the original simulation (black), interpolated BioMime transformations (blue) and extrapolated BioMime transformations beyond the specified conditions in the training set with colour set by euclidean distance from these conditions. The distribution of the interpolated MUAPs closely matched those from the original simulation, whilst the extrapolated emissions only started to deviate at relative distances greater than 60% from the ranges of specified conditions in the training set.

protocols for sEMG recordings. Finally, the individual MU activities for each electrode channel were summed to give the final sEMG activity (Fig. 5e). This full-spectrum simulation is prohibitively time-consuming using numerical methods due to the complicated pre-processing steps and the computational cost of simulating hundreds of MUAPs at discretised stages of the movement. By contrast, it took less than two minutes for BioMime to simulate the same amount of data.

Discussion

Humans are in nature dynamic systems. Computationally-feasible methods are needed to better reflect this fact in biophysical simulations. By transferring the knowledge of numerical simulations to a conditional generative model, we demonstrate that the cost associated with simulating an evolving biophysical system can be largely mitigated without losing the prediction fidelity. With the correct architecture design, such models can double both as a rapid way to transform existing simulation emissions to reflect new system states and as *de novo* generators for new emissions.

An example of a conditional generative model, BioMime, was demonstrated to generalisably and accurately learn the outputs of a teacher numerical simulator. Such advanced numerical simulators are commonly defined by a large number of differential equations which describe a complex system. BioMime was further able to continuously interpolate between the system states of the numerical simulator. This allows a rapid and robust generation of dynamic biophysical emissions that closely tracked those of the teacher finite element method-based simulation. In practice, generating the required emissions by BioMime was two orders of magnitude faster than by the numerical simulator. This efficiency allows us to demonstrate the first practical model for simulating the

myoelectric output of a moving forearm during a realistic hand and wrist movement. In the field of neurophysiological signal decomposition, there is a clear need for such simulations that capture the effect of dynamic changes to the volume conductor, which has so far proved a bottleneck to the development and validation of source separation algorithms that can operate on this highly non-stationary signal (23). The proposed methodology goes some way in meeting such a demand.

The main disadvantage of using a conditional generative model for simulation is that it is reliant on the quality and quantity of the training emissions, although this is the case with any method of supervised or unsupervised machine learning. BioMime was trained on the dataset generated by an advanced numerical forearm model with a few condition changes. Since only one 3D model was included, BioMime embeds the specific features of this forearm model into the unspecified conditions, as a “digital twin” of the individual’s forearm. Thus, the synthesised outputs are closely clustered with the samples in the original dataset. When more subject’s models are available in the dataset, the variance of the unspecified conditions increases. We would expect that BioMime will capture the variance and embed the variance to the latent features, as we have shown by the informativeness score that with the current training pipeline, the model is able to disentangle the specified conditions and the unspecified ones. Therefore, BioMime is potentially flexible to capture the features of the biophysical system from specific to general given the corresponding datasets.

There is no requirement that BioMime be trained on the emissions of only one system. Here, we showed a feasible implementation of multi-domain simulation by feeding BioMime with the outputs of a musculoskeletal model during dynamic movements. This enables the exploration of neuromusculoskeletal mechanisms from both bioelectrical and biomechanical per-

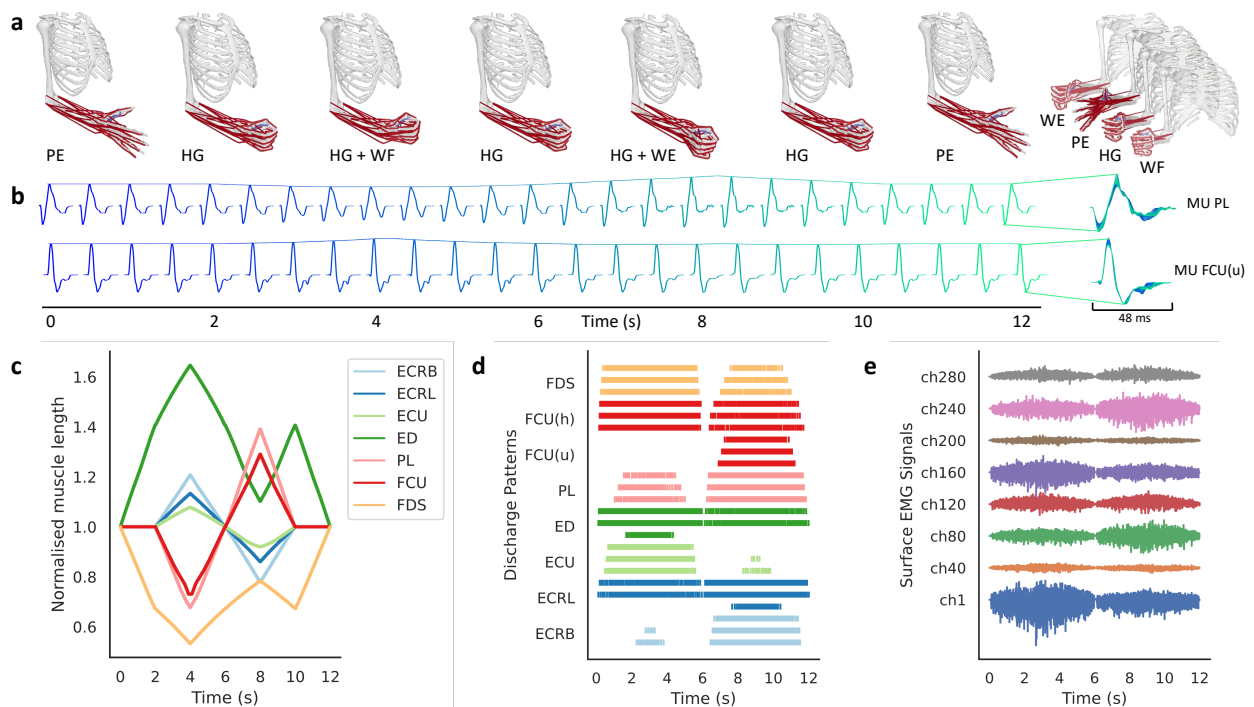


Fig. 5. BioMime can be used to mimic the dynamic changes of a biophysical system that matches the mechanical movements of a musculoskeletal model. a. Sequence of the movements. PE, palm extension; HG, hand grasp; WF, wrist flexion; WE, wrist extension. **b.** Two representative MUAPs generated by BioMime, which are continuously morphed using the muscle length profiles given by the musculoskeletal model. The upper MUAP is from Palmaris longus, PL and the lower MUAP is from the ulnar head of Flexor carpi ulnaris, FCU(u). The lines that connect the peak of MUAPs show the changes in MUAP amplitude. The MUAPs do not show extreme variations. This is expected as only one specified condition, the muscle length, is changed during the transformation. **c.** Normalised muscle length profiles from the musculoskeletal model. ECRB, Extensor carpi radialis brevis; ECRL, Extensor carpi radialis longus; ECU, Extensor carpi ulnaris; ED, Extensor digitorum; PL, Palmaris longus; FCU, Flexor carpi ulnaris (ulnar head and humeral head); FDS, Flexor digitorum superficialis. **d.** Representative discharge patterns of three motor units in each muscle. **e.** Simulated surface EMG signals in eight channels. This complex dynamic simulation is only possible due to the low computational cost of the hundreds of MUAP transformations conducted by BioMime. Details of the musculoskeletal model are described in *Methods*.

spectives, the first step to integratively studying motoneuron activities and the movements driven by these activities (7). The computational burden of such full-spectrum simulations of biophysical systems is massive, which precludes the modelling of a range of movements with small time steps. However, this becomes possible by training conditional generative models like BioMime to effectively merge the emissions of the component simulations. Another application is to use BioMime as a surrogate forward model in an end-to-end optimisation pipeline (29). When the electrical generation process takes part in a larger-scale modelling, for example simulation from the cell activity to the electric potential field, a differentiable and computationally efficient forward model is required for an end-to-end optimisation. BioMime provides a promising solution to approximating this complicated forward process.

It is important to emphasise that the methods outlined in this paper are designed to augment and approximate, rather than replace, high-quality numerical modelling. In many biophysical domains, the dynamic changes in system parameters in response to some perturbations remain poorly characterised, which restricts the utility of BioMime for simulating such systems. This is particularly true when modelling dynamic changes in a volume conductor for generating sEMG signals. While we attempted to carefully estimate the likely parameter changes during a forearm movement by using the musculoskeletal model, only muscle lengths can be tracked, which limits the precise restoration of MUAP changes. There is also a

dearth of such information in the literature. We hope that the promise offered by conditional generative models in capturing the dynamic systems will further stimulate research in this direction, which will in turn improve the generation accuracy of BioMime.

Contemporary methods of biophysical simulation continue to offer a range of opportunities to both test physiological hypotheses and as a test bed for medical technologies. High representational-capacity generative modelling, such as the methods described in this paper, offers an enormously flexible opportunity for leveraging the domain knowledge contained within these complex systems. We anticipate that the pipeline of a back-end numerical model and a front-end generative model will become increasingly common in future simulation design, and we look forward to the corresponding expansion in dynamic simulation that these techniques will enable.

Methods

Model Architecture. The proposed deep latent variable model, BioMime, takes the form of a probabilistic autoencoder architecture with an encoder and decoder network (Supplementary Table 1). The encoder network consists of five convolutional layers, each of which includes a 3D convolution with kernel size 3 followed by a 1×1 convolution with a skip connection. A parametric rectified linear unit activation (PReLU) operation is performed after each convolution layer. The convolutional output is then flattened and passed to two linear layers, which

estimate the sufficient statistics of the approximate posterior, mean and variance, respectively. During training, the approximate posterior is sampled by the reparameterisation trick. During inference, the expectation of the posterior is used as the latent representation (Supplementary Algorithm 2) for transforming the input samples, whilst for *ab initio* generation, the latents are taken from a gaussian prior with zero mean and identity covariance (Supplementary Algorithm 3). The latent representation is then concatenated with a 64-dimensional learned linear projection of the six specified conditions before being passed to the decoder.

The decoder consists of four convolutions followed by two upscaling blocks. Each upscaling block consists of a time-scaling module, a 3D convolution, and a 1×1 convolution in sequence. The time-scaling module is a mean pooling/unpooling bank with learned weights (Supplementary Fig. 1), specialised for dilating or compressing the time sequences, which is essential in modelling physiological signals but computationally expensive to achieve through many convolutional operations. Inspired by the dynamic convolution in (30) and the multi-scale spatial pooling in (31), the time-scaling module uses a series of experts e_k with different scaling factors to dilate or compress the inputs, conditioned on the specified conditions \mathbf{c}_s . The contribution of each expert is modulated by a scalar weight, which is the output of a three-layer multilayer perceptron with the six specified conditions as input:

$$\begin{aligned} \mathbf{y} &= \sum_k \pi_k(\mathbf{c}_s) e_k(\mathbf{x}) \\ \text{s.t. } 0 &\leq \pi_k(\mathbf{c}_s) \leq 1, \sum_k \pi_k(\mathbf{c}_s) = 1 \end{aligned} \quad [1]$$

where $\pi_k(\mathbf{c}_s)$ is the weight of the k th expert conditioned on the desired states \mathbf{c}_s . In this study, we used eight experts with scaling factors linearly spaced from 0.25 to 2.0, which showed optimal performance in both convergence and reconstruction accuracy (Supplementary Fig. 4).

Training Pipeline. Whilst BioMime has a deep latent variable architecture similar to a VAE, it is not trained variationally. Instead we found that a conditional adversarial method gave the best performance. The output of BioMime is inspected by a conditional discriminator network of the similar architecture as the encoder, trained to identify whether samples are from the original dataset or generated by BioMime. Conditioning was performed by concatenating the output of the first convolutional layer with the specified conditions.

The goals of training BioMime are to 1) produce novel data samples that are realistic enough to fool the discriminator and 2) enable generation by both sampling from a prior distribution and by encoding an existing emission. These are achieved by optimising the following objective function:

$$\mathcal{L}_G = \lambda_1 \mathcal{L}_{GAN} + \lambda_2 \mathcal{L}_{KL} + \lambda_3 \mathcal{L}_{cyclic} \quad [2]$$

The first term \mathcal{L}_{GAN} is an adversarial loss, which evaluates the performance of BioMime using the conditional discriminator. The second term \mathcal{L}_{KL} is the Kullback-Leibler divergence ($\mathcal{D}_{KL}(\cdot||\cdot)$) between the predicted distribution of the latent feature and the standard normal distribution $\mathcal{N}(0, 1)$. Minimizing \mathcal{L}_{KL} regularises the latent space to approach $\mathcal{N}(0, 1)$. This enables the model to generate new data by sampling from the prior. An additional cycle-consistency loss \mathcal{L}_{cyclic}

is included to improve training stability and generation accuracy (Supplementary Fig. 4), which is the mean-squared error between the input sample and the reversed sample (Fig. 1b). In our experiments, the hyper-parameters λ_1 was set 10, λ_2 was an annealing weight (32) increased from 0 to 0.05 in 30,000 iterations, and λ_3 was set 0.5. Comparisons of constant, logistic, and linear KL divergence schedules are shown in Supplementary Fig. 4.

The objective of the discriminator is to differentiate the data samples produced by the generator from those in the original dataset whilst also detecting whether the samples match the specific conditions. This is done by minimising:

$$\begin{aligned} \mathcal{L}_D &= -\mathbb{E}_{\mathbf{x}}[\log D(\mathbf{x}, \mathbf{c}_s)] \\ &\quad -\mathbb{E}_{\mathbf{x}}[\log(1 - D(\mathbf{x}, \mathbf{c}_r))] * 0.5 \\ &\quad -\mathbb{E}_{\mathbf{x}}[\log(1 - D(G(\mathbf{x}, \mathbf{c}_s), \mathbf{c}_s))] * 0.5 \end{aligned} \quad [3]$$

In this way, the discriminator only predicts an input as real when the sample \mathbf{x} is realistic and matches the desired conditions \mathbf{c}_s . Real samples \mathbf{x} with random conditions \mathbf{c}_r or synthesised samples $G(\mathbf{x}, \mathbf{c}_s)$ with matched conditions \mathbf{c}_s are predicted as fake.

Training Process The ratio between the discriminator and the generator updates was set 1 : 1 (Supplementary Algorithm 1). The discriminator and the generator were trained for 45 epochs (405,000 iterations) with RMSprop optimiser and learning rate of 1×10^{-5} . The number of input signals in each training mini-batch was set to 32. Training took 120 hours (~5 days) on a NVIDIA RTX 2080Ti.

Data Preparation. We used an advanced finite element-based numerical model with a realistic forearm anatomy provided by the Neurodec software (22) to prepare the dataset of simulation emissions (Supplementary Methods and Supplementary Fig. 2). To simulate the motor unit action potentials with sufficient variation of conditions, a total of 1,500 motor units were randomly generated within the eight forearm muscles, including the superficial muscles in the flexors and extensors. Each motor unit controlled a bundle of muscle fibres that clustered within a sub-volume of the muscle (Fig. 2). Six factors of variations that explained the bulk of MUAPs were defined as the specified conditions, covering the properties of current sources, motor units, and the volume conductor.

For each MU, the action potential templates under 256 conditions were generated, which were the combinations of four fibre densities (200, 266, 333, 400 fibres per mm^2), four current source propagation velocities (3.0, 3.5, 4.0, 4.5 m/s), four neuromuscular junction positions (0.4, 0.46, 0.53, 0.6), and four fibre lengths in ratio (0.85, 0.95, 1.05, 1.15). Note that rather than directly using the fibre density as one of the conditions, we used the number of muscle fibres in each MU, such that this condition changed more continuously. The other two specified conditions are the depth and the medial-lateral position of the MU centre, which was defined as the geometric centre of all the muscle fibres it controlled. The six specified conditions were linearly normalised between 0.5 and 1. The influences of the six conditions on the MUAP attributes are visualised in Supplementary Fig. 3.

There were a total of 384,000 samples in the dataset. Considering that the most unseen conditions come with different

motor unit locations, we divide the dataset into the training dataset and the testing dataset by the motor units. For each muscle, 75% of MUs were randomly selected as the training set (288,000 samples) and the others as the held-out test set (96,000 samples). The MUAP templates were simulated with a bracelet of 10×32 electrodes with inter-electrode distance of 8 mm, which covered the bellies of the forearm muscles. The templates were represented as matrices with size $10 \times 32 \times T$. The number of time samples T varied among muscles due to the different fibre lengths and the current source propagation velocities. During the preprocessing of the MUAP data, the signals were first downsampled to 2,000 Hz and were centered with their accumulative power. Finally, the signals were cut to a common length of 96 temporal samples (48 ms).

Model Validation. To validate the model, we evaluated the ability of BioMime to transform the existing MUAP templates to new sets of simulation parameters. This was performed by optimising the model on the training dataset and evaluating its performance on the held-out test set. We randomly selected two data samples with the same unspecified generative factors and transformed the first sample to match the second sample's specified conditions. The generation accuracy was evaluated by the normalised root mean square between the predicted MUAP and the ground truth MUAP.

Musculoskeletal Model. To simulate MUAPs and the accumulated muscle activities during a realistic movement, we fed BioMime with a sequence of continuously changed physiological parameters. The length of each muscle was computed by an open-source musculoskeletal model (33) with a hand, wrist, and forearm in OpenSim (34). The model includes 23 independent degrees of freedom and 43 hill-type muscle-tendon actuators that represent the intrinsic muscles of the hand, the extrinsic muscles of the hand, and the primary wrist muscles. We defined four gestures, palm extension (PE), hand grasp (HG), wrist flexion (WF), and wrist extension (WE) by setting the joint angles. The musculoskeletal model was driven by the interpolated joint angles. Starting from the gesture of palm extension, the model performed the following (combinations of) gestures in sequence: hand grasp, hand grasp and wrist flexion, hand grasp, hand grasp and wrist extension, hand grasp, and palm extension. Each movement took 2 seconds, thus 12 seconds in total. The profiles of equilibrium muscle lengths were computed at 50 Hz frequency. The muscle lengths were first normalised to the lengths at the start position (PE) before fed into BioMime to simulate dynamic MUAP waveforms.

Informatic Analyses.

Normalised root mean square error To quantify the accuracy of the generated signals compared with the ground truth, the normalised root mean square error was used as a metric:

$$\text{nRMSE} = \frac{\sqrt{\sum_{h,w,t} (x_{h,w,t} - \tilde{x}_{h,w,t})^2 / H/W/T}}{x_{max} - x_{min}} \quad [4]$$

where x and \tilde{x} indicate the ground truth MUAP from the numerical model and the synthesised MUAP by BioMime. The variables h , w , t are the summation over the rows and columns of the electrode and the time samples, with the total

number H , W , and T , respectively. x_{max} and x_{min} are the maximum and minimum values of the sample. The normalised root mean square error is often expressed as a percentage, with a lower value indicating a less residual variance for the model and a higher generation accuracy. We empirically found that a nRMSE less than 2.0% indicates a good generation with few differences between the generated data and the ground truth data.

t-distributed stochastic neighbor embedding (t-SNE)

To visualise the implicit structure of the MUAP data, we used t-SNE to project the signals to a low-dimensional submanifold. The scikit-learn t-SNE module was used with default settings (dimension of the embedded space 2, perplexity 30, learning rate 200, maximum number of iterations 1000, initialization of embedding using principle component analysis) (35). The samples were visualised in the coordinates given by t-SNE, where similar samples were close together in the submanifold.

Informativeness score We explored the amount of information of the specified conditions embedded in the latent representations of the generator. The informativeness of the latent vector \mathbf{z} about the i th generative factor \mathbf{c}_{s_i} can be quantified by the prediction accuracy $P(\mathbf{c}_{s_i}, f(\mathbf{z}))$, where P is an accuracy metric and f is a regressor (26). The informativeness depends on 1) the regressor's capability to extract information from the latent representations and 2) the way the specified conditions are embedded in the latent features, e.g., disentanglement of the specified conditions in the representations will make the regression easier.

We used multilayer perceptron with non-linear activation functions to predict \mathbf{c}_{s_i} from \mathbf{z} . The prediction accuracy was measured as the percentage of correctly predicted samples. A sample was regarded as correct when the relative error between the predicted and real conditions was within a threshold. For instance, with the threshold of 0.05, a sample with ground truth condition a will be evaluated as correct if the predicted condition is between $0.95a \sim 1.05a$. We chose ten threshold levels, linearly spaced from 0.01 to 0.10, and calculated the average accuracy as the informativeness score (Supplementary Table 2).

Code availability

All code was implemented in Python using the deep learning framework PyTorch. Code which implements the models used in this paper is available at <https://github.com/shihanna/BioMime> and is provided under the GNU General Public License v3.0.

ACKNOWLEDGMENTS. We would like to thank Pranav Mami-danna for the discussions and assistance in preparing the musculoskeletal model. This study is supported by the National Natural Science Foundation of China (Grant No. 91948302, 52175021), the European Research Council Synergy Grant NaturalBionicS (contract 810346), the EPSRC Transformative Healthcare, NISNEM Technology (EP/T020970), and the BBSRC, "Neural Commands for Fast Movements in the Primate Motor System" (NU-003743).

1. W Gerstner, H Sprekeler, G Deco, Theory and simulation in neuroscience. *science* **338**, 60–65 (2012).
2. E Hallilaj, et al., Machine learning in human movement biomechanics: Best practices, common pitfalls, and new opportunities. *J. biomechanics* **81**, 1–11 (2018).
3. AL Hodgkin, AF Huxley, A quantitative description of membrane current and its application to conduction and excitation in nerve. *The J. physiology* **117**, 500 (1952).
4. M Breakspear, Dynamic models of large-scale brain activity. *Nat. neuroscience* **20**, 340–352 (2017).

5. D Baby, A Van Den Broucke, S Verhulst, A convolutional neural-network model of human cochlear mechanics and filter tuning for real-time applications. *Nat. machine intelligence* **3**, 134–143 (2021).
6. M Fuchs, R Drenckhahn, H Wischmann, M Wagner, An improved boundary element method for realistic volume-conductor modeling. *IEEE Transactions on biomedical engineering* **45**, 980–997 (1998).
7. V Caggiano, H Wang, G Durandau, M Sartori, V Kumar, Myosuite: A contact-rich simulation suite for musculoskeletal motor control in *Learning for Dynamics and Control Conference*. (PMLR), pp. 492–507 (2022).
8. D Pereira Botelho, K Curran, MM Lowery, Anatomically accurate model of emg during index finger flexion and abduction derived from diffusion tensor imaging. *PLoS computational biology* **15**, e1007267 (2019).
9. A Erdemir, Open knee: open source modeling and simulation in knee biomechanics. *The journal knee surgery* **29**, 107–116 (2016).
10. S Numata, et al., Blood flow analysis of the aortic arch using computational fluid dynamics. *Eur. J. Cardio-Thoracic Surg.* **49**, 1578–1585 (2016).
11. MN Kamel Boulos, P Zhang, Digital twins: from personalised medicine to precision public health. *J. Pers. Medicine* **11**, 745 (2021).
12. F Zhuang, et al., A comprehensive survey on transfer learning. *Proc. IEEE* **109**, 43–76 (2020).
13. Y Pu, et al., Variational autoencoder for deep learning of images, labels and captions. *Adv. neural information processing systems* **29** (2016).
14. X Yan, J Yang, K Sohn, H Lee, Attribute2image: Conditional image generation from visual attributes in *European conference on computer vision*. (Springer), pp. 776–791 (2016).
15. NW Gebauer, M Gastegger, SS Hessmann, KR Müller, KT Schütt, Inverse design of 3d molecular structures with conditional generative neural networks. *Nat. communications* **13**, 1–11 (2022).
16. R Merletti, D Farina, *Surface electromyography: physiology, engineering, and applications*. (John Wiley & Sons), (2016).
17. D Farina, et al., The extraction of neural information from the surface emg for the control of upper-limb prostheses: emerging avenues and challenges. *IEEE Transactions on Neural Syst. Rehabil. Eng.* **22**, 797–809 (2014).
18. V Ruonala, et al., Emg signal morphology and kinematic parameters in essential tremor and parkinson's disease patients. *J. Electromyogr. Kinesiol.* **24**, 300–306 (2014).
19. TS Saponas, DS Tan, D Morris, R Balakrishnan, Demonstrating the feasibility of using forearm electromyography for muscle-computer interfaces in *Proceedings of the SIGCHI Conference on Human Factors in Computing Systems*. pp. 515–524 (2008).
20. D Xiong, D Zhang, X Zhao, Y Zhao, Deep learning for emg-based human-machine interaction: a review. *IEEE/CAA J. Autom. Sinica* **8**, 512–533 (2021).
21. D Farina, F Negro, M Gazzoni, RM Enoka, Detecting the unique representation of motor-unit action potentials in the surface electromyogram. *J. neurophysiology* **100**, 1223–1233 (2008).
22. K Maksymenko, AK Clarke, IM Guerra, S Deslauriers-Gauthier, D Farina, Towards the myoelectric digital twin: Ultra fast and realistic modelling for deep learning. *bioRxiv* pp. 2021–06 (2022).
23. V Glaser, A Holobar, Motor unit identification from high-density surface electromyograms in repeated dynamic muscle contractions. *IEEE Transactions on Neural Syst. Rehabil. Eng.* **27**, 66–75 (2018).
24. PK Gyawali, Z Li, S Ghimire, L Wang, Semi-supervised learning by disentangling and self-ensembling over stochastic latent space in *International Conference on Medical Image Computing and Computer-Assisted Intervention*. (Springer), pp. 766–774 (2019).
25. T Wang, Z Yue, J Huang, Q Sun, H Zhang, Self-supervised learning disentangled group representation as feature. *Adv. Neural Inf. Process. Syst.* **34**, 18225–18240 (2021).
26. C Eastwood, CK Williams, A framework for the quantitative evaluation of disentangled representations in *International Conference on Learning Representations*. (2018).
27. L Van der Maaten, G Hinton, Visualizing data using t-sne. *J. machine learning research* **9** (2008).
28. MM Lowery, NS Stoykov, JP Dewald, TA Kuiken, Volume conduction in an anatomically based surface emg model. *IEEE Transactions on Biomed. Eng.* **51**, 2138–2147 (2004).
29. D Montes de Oca Zapaiain, JA Stewart, R Dingreville, Accelerating phase-field-based microstructure evolution predictions via surrogate models trained by machine learning methods. *npj Comput. Mater.* **7**, 1–11 (2021).
30. Y Chen, et al., Dynamic convolution: Attention over convolution kernels in *Proceedings of the IEEE/CVF Conference on Computer Vision and Pattern Recognition*. pp. 11030–11039 (2020).
31. JW Chen, et al., A convolutional neural network with parallel multi-scale spatial pooling to detect temporal changes in sar images. *Remote. Sens.* **12**, 1619 (2020).
32. SR Bowman, et al., Generating sentences from a continuous space. *arXiv preprint arXiv:1511.06349* (2015).
33. DC McFarland, et al., A musculoskeletal model of the hand and wrist capable of simulating functional tasks. *IEEE Transactions on Biomed. Eng.* (2022).
34. SL Delp, et al., Opensim: open-source software to create and analyze dynamic simulations of movement. *IEEE transactions on biomedical engineering* **54**, 1940–1950 (2007).
35. F Pedregosa, et al., Scikit-learn: Machine learning in Python. *J. Mach. Learn. Res.* **12**, 2825–2830 (2011).